Electronic Supplementary Material (ESI) for Nanoscale.
This journal is © The Royal Society of Chemistry 2017

Supporting Information

Identification of pH-dependent synergy on Ru/MoS_2 interface: a comparison of alkaline and acidic hydrogen evolution

Jinlong Liu,[a] Yao Zheng,[a] Dongdong Zhu,[a] Anthony Vasileff,[a] Tao Ling[b] and Shi-Zhang Qiao*[ab]

[a]School of Chemical Engineering, University of Adelaide, Adelaide, SA 5005, Australia. [b]School of Materials Science and Engineering, Tianjin University, Tianjin 300072, China

Corresponding Author: Shi-Zhang Qiao, E-mail address: s.qiao@adelaide.edu.au

1. Experimental Section

1.1 Materials

All chemicals (analytical reagent grade) used in this work, including $(NH_4)_6Mo_7O_{24}\cdot 4H_2O$, $NaH_2PO_2\cdot 4H_2O$, thiourea, urea, KOH, H_2SO_4, Pt/C (20 wt.% of Pt on Vulcan XC72), Nafion (15 wt.%) were purchased from Sigma-Aldrich and used without further purification. Carbon paper (CP, AvCarb MGL 190, Product Code: 1594008) was bought from FuelCellStore. Ultra-pure water (18.2 MΩ·cm, PURELAB Option-Q) was used in all experiments.

1.2 Synthesis of Electrocatalysts

***Preparation of MoS_2/CP*:** A piece of CP (2 cm × 4 cm) was washed thoroughly with ethanol, 0.5 M H_2SO_4, and water in sequence under sonication for 1 h each time. The vertically aligned MoS_2 nanosheets were grown on the cleaned CP via a facile hydrothermal approach. Typically, $(NH_4)_6Mo_7O_{24}\cdot 4H_2O$ (0.088 g), thiourea (0.163 g), $NaH_2PO_2\cdot 4H_2O$ (0.023 g) were added into 35 mL of deionized water under magnetic stirring to obtain a precursor solution, which was then transferred to a Teflon-lined stainless autoclave (50 mL) with a piece of pre-cleaned CP. Subsequently, the autoclave was kept in a preheated oven at 180 ºC for 24 h. After the autoclave cooled down naturally to ambient temperature, the sample was collected and rinsed with deionized water several times, and then dried in a vacuum oven at 60 ºC overnight.

***Preparation of Ru/MoS_2/CP*:** The obtained MoS_2/CP was completely immersed into 20 mL of $RuCl_3$ aqueous solution (5 mM) for 24 h. The product was collected and dried using compressed N_2 at ambient temperature. To obtain the final product, the sample was then heated to 250 ºC in a tube furnace at a rate of 2 ºC min^{-1} and held at that temperature for 2 h under H_2/Ar flow. For the as-prepared Ru/MoS_2/CP, the mass increment of CP was about 1.0 mg cm^{-2}. XPS quantification analysis revealed that the atomic percentage of Ru in Ru/MoS_2 was ~15 at.%, which converts to a Ru mass percentage of about 10%. Accordingly, the Ru loading for Ru/MoS_2/CP was ~0.1 mg cm^{-2}.

***Preparation of MoS_2*:** Bare MoS_2 was synthesized via a hydrothermal approach similar to that of MoS_2/CP. Specifically, $(NH_4)_6Mo_7O_{24}\cdot 4H_2O$ (1.236 g), thiourea (2.284 g), $NaH_2PO_2\cdot 4H_2O$ (0.318 g) were added into 35 mL of deionized water under magnetic stirring to obtain a precursor solution, which was then transferred to a Teflon-lined stainless autoclave (50 mL) without CP. Subsequently, the autoclave was kept in a preheated oven at 180 ºC for 24 h. After the autoclave cooled down naturally to ambient temperature, the resultant precipitates were

collected by centrifugation, washed with deionized water several times, and then dried in a vacuum oven at 60 ºC overnight.

***Preparation of Ru/CP*:** A piece of pre-cleaned CP was completely immersed in 20 mL of $RuCl_3$ aqueous solution (5 mM) for 24 h. The following procedure was the same as the preparation of $Ru/MoS_2/CP$. For the as-prepared Ru/CP, the mass increment of CP was ~0.31 mg cm^{-2}, which was attributed to the Ru loading.

***Preparation of PtC/CP*:** 5 mg of 20 wt.% Pt/C was dispersed in 2 mL of ethanol containing 0.15 wt.% of Nafion under ultrasound for 1 h. Next, 200 μL of the Pt/C dispersion was loaded onto a piece of pre-cleaned CP (1 cm × 1 cm) to obtain the PtC/CP electrode.

1.3 Characterizations

The morphology, structure, and chemical composition of the samples were characterized by field emission scanning electron microscopy (SEM, QUANTA 450) equipped with energy dispersive spectrometer (EDS), transmission electron microscopy (TEM, Tecnai G2 Spirit and JEOL 2100 Cryo) equipped with EDS, powder X-ray diffractometer (XRD, Cu-target Bruker D8 Advance), X-ray photoelectron spectroscopy (XPS, ESCALab250).

1.4 Electrochemical Measurements

Electrochemical measurements were performed on a 760D (CH Instruments, Inc., USA) in a standard three-electrode glass cell (Pine Research Instruments, USA). 1 cm × 1 cm $Ru/MoS_2/CP$, MoS_2/CP, Ru/CP, and PtC/CP were directly used as the working electrode. For MoS_2, a glassy carbon rotating disk electrode (RDE, diameter: 5 mm) was employed. Specifically, 5 mg of MoS_2 was dispersed in 2 mL of ethanol containing 0.15 wt.% of Nafion under sonication for 1 h. 40 μL of the catalyst ink (2 mg mL^{-1}) was loaded onto the RDE (0.196 cm^2) serving as the working electrode. A carbon rod and an Ag/AgCl (4 M KCl) electrode were used as the counter electrode and the reference electrode, respectively. All potentials were referenced to the reversible hydrogen electrode (RHE) using the following equation: E(RHE) = E(Ag/AgCl) + 0.205 + 0.059 × pH. All the electrolytes were purged with N_2 for 30 min before measurements to remove dissolved O_2. The linear sweep voltammetry (LSV) curves were collected with a scan rate of 5 mV s^{-1}. Electrochemical impedance spectroscopy (EIS) was measured in the frequency range from 0.1 Hz to 100 kHz with an amplitude of 5 mV. The double-layer capacitance (C_{dl}) and roughness factor (R_f) of various samples were evaluated from the capacitance of the double-layer at the electrode-electrolyte interface using cyclic voltammetry (CV) in a small potential range of 0.15−0.25 V vs. RHE. IR compensation of

polarization curves was performed using the solution resistance (R_s) estimated from EIS measurements. The long-term stability test was carried out by chronoamperometric measurement and repetitive CV scans in a potential window from 0 to −0.35 V vs. RHE (refer to IR-uncompensated values). The evolved H_2 was analyzed using gas chromatograph (GC, Clarus 480, PerkinElmer, USA with Ar as a carrier gas and 5 Å molecular sieve column).

2. Supplementary Figures

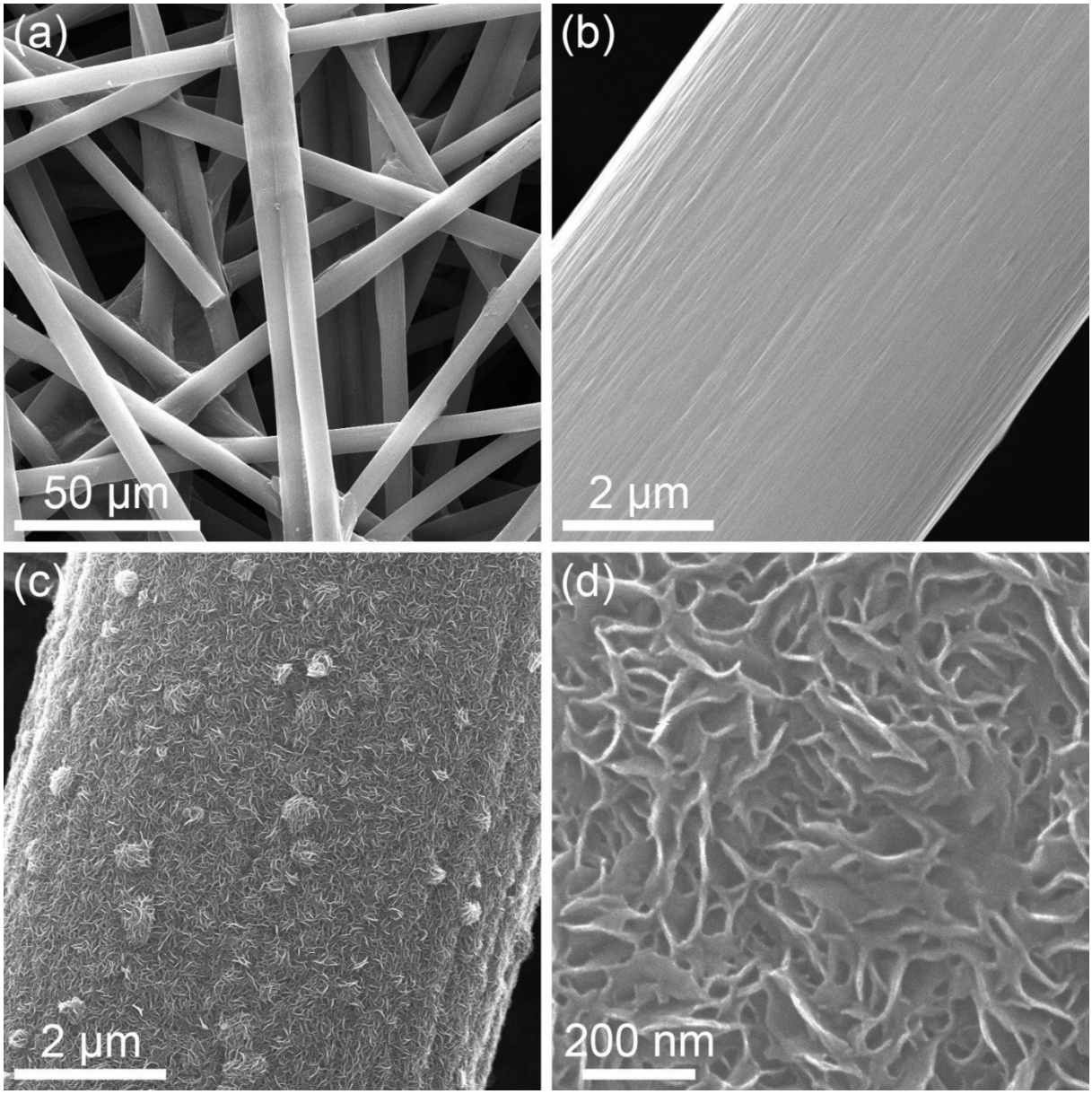

Fig. S1 (a,b) SEM images of pre-cleaned carbon paper (CP) with clean surface. (c,d) SEM images of MoS_2/CP, showing the full and homogeneous coverage of CP by vertically aligned MoS_2 nanosheets.

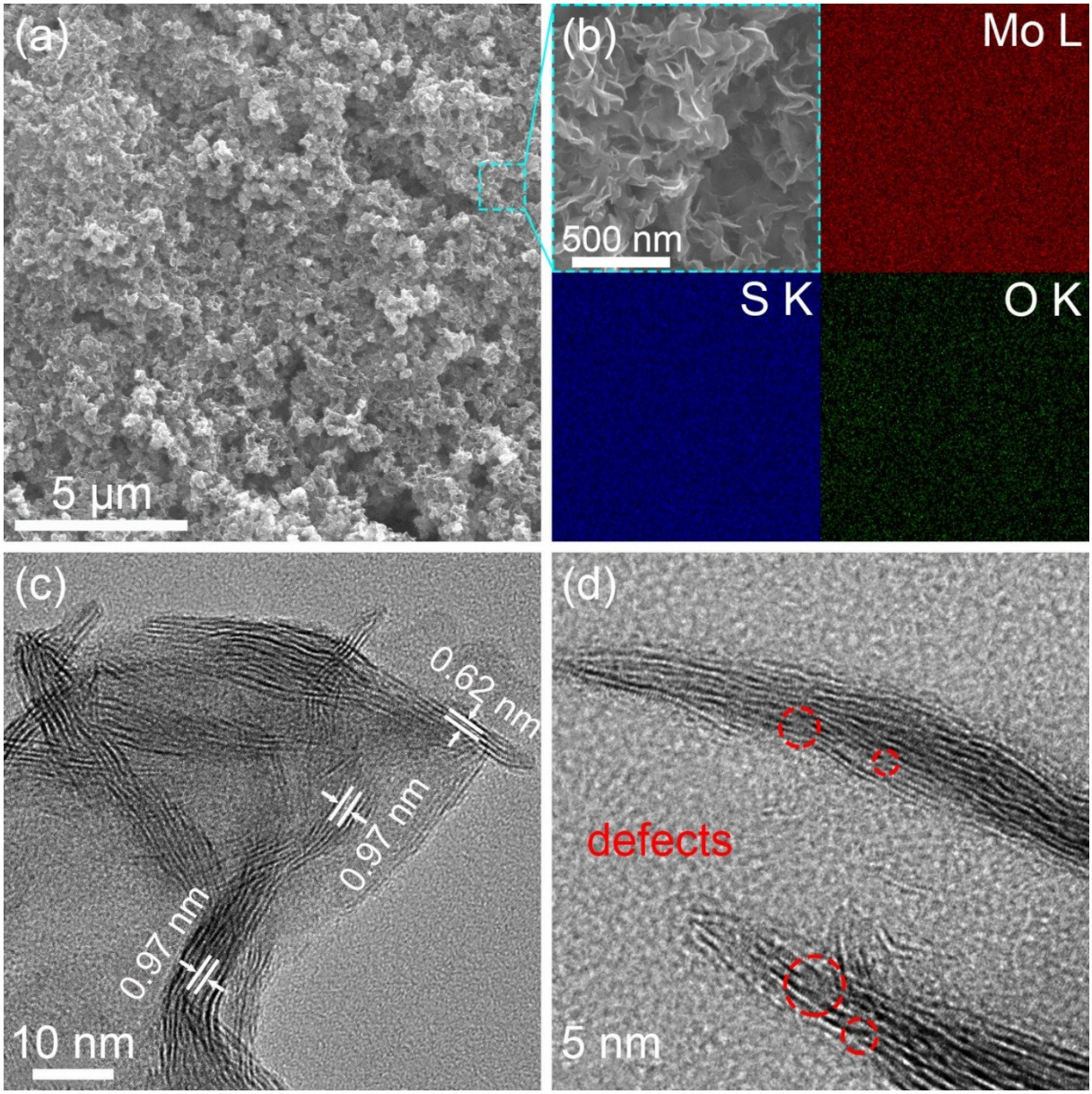

Fig. S2 (a) SEM image of MoS_2. (b) Magnified SEM image and corresponding element mapping of MoS_2 for the selected area. (c) HRTEM image of few-layer MoS_2 nanosheets. The well-defined interplanar distance of 0.62 nm corresponds to (002) planes of hexagonal MoS_2, while the large distance of 0.97 nm indicates the appearance of enlarged interlayers, which agrees with previous reports.[1] (d) Cross-sectional HRTEM image of MoS_2 nanosheets. Selected areas, indicated by red dashed circles, show the presence of defects in the MoS_2 nanosheets.

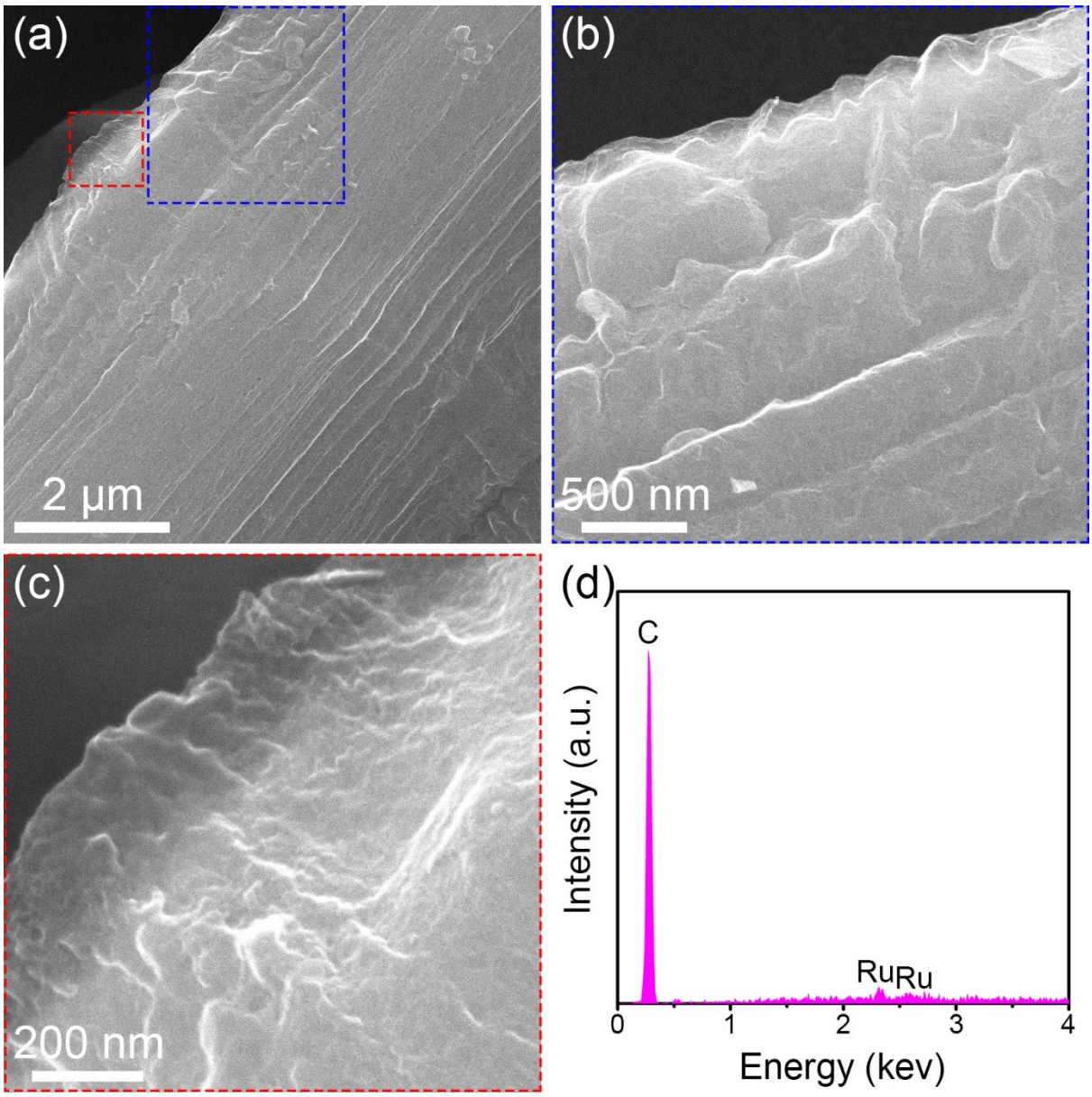

Fig. S3 (a) SEM image of Ru/CP. (b,c) Magnified SEM images of Ru/CP for selected areas, showing the wrinkled Ru on CP. (d) EDS spectrum of Ru/CP containing C and Ru.

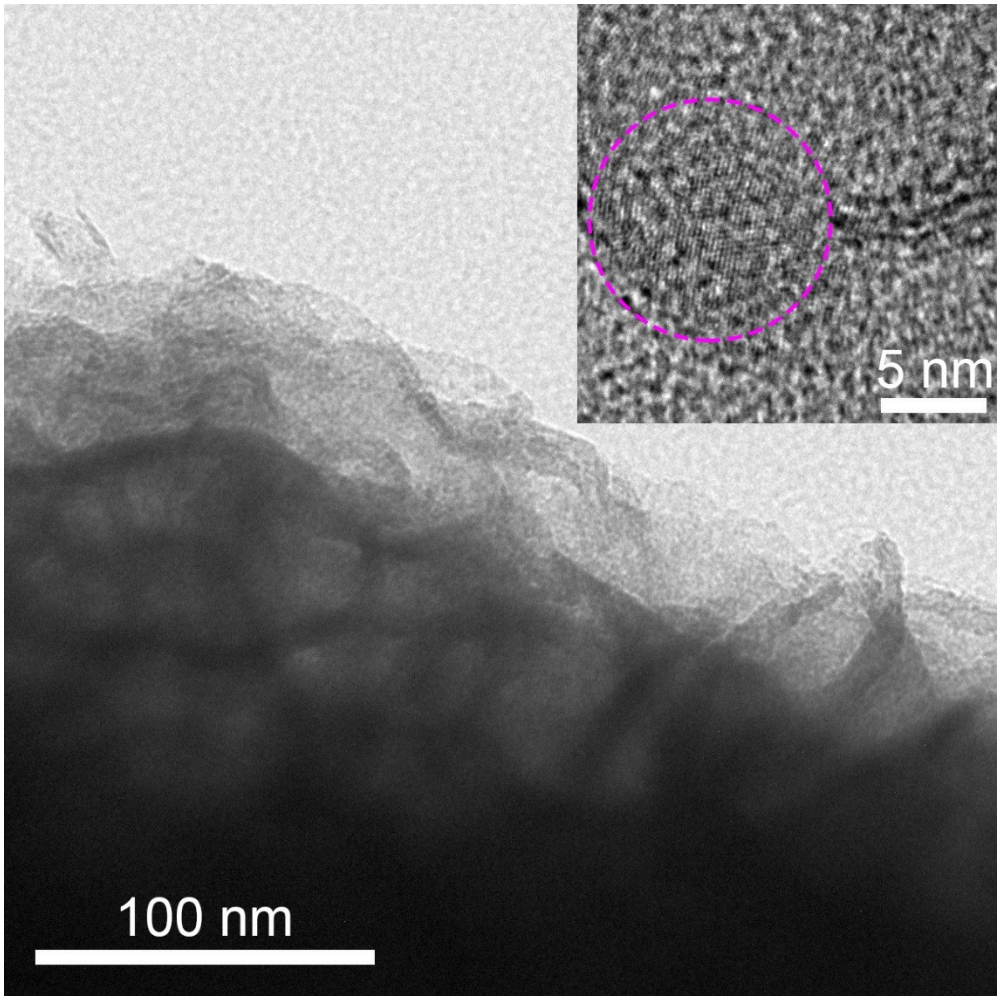

Fig. S4 TEM image of Ru/MoS_2. Inset HRTEM image shows an individual Ru nanoparticle of about 10 nm in size.

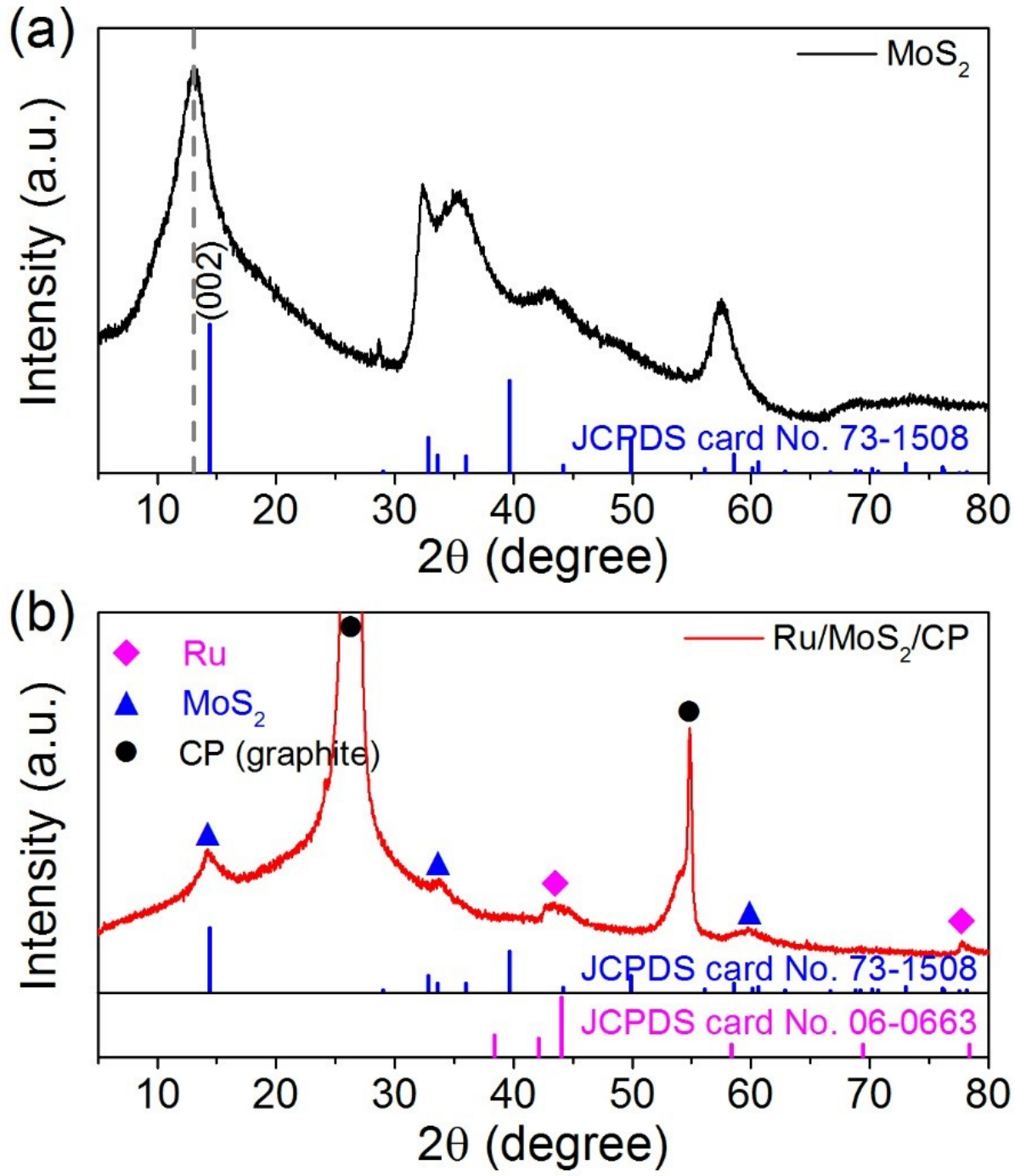

Fig. S5 XRD patterns of (a) bare MoS_2 and (b) Ru/MoS_2/CP. The standard patterns of the hexagonal MoS_2 (JCPDS card No. 73-1508) and the hexagonal Ru (JCPDS card No. 06-0663) are given as references. In the XRD pattern of bare MoS_2, the shift of the (002) peak to a lower angle indicates the expansion of partial interlayers, matching well with HRTEM observation (Fig. S2c). According to Xie et al.'s report, thermal treatment (> 232 ºC) could lead to a structural conversion to the thermodynamically stable 2H-MoS_2.[1] For this reason, the XRD pattern of Ru/MoS_2/CP shows no shift of the (002) peak of MoS_2, which can be further confirmed by its HRTEM result without enlarged interlayers (Fig. 1d).

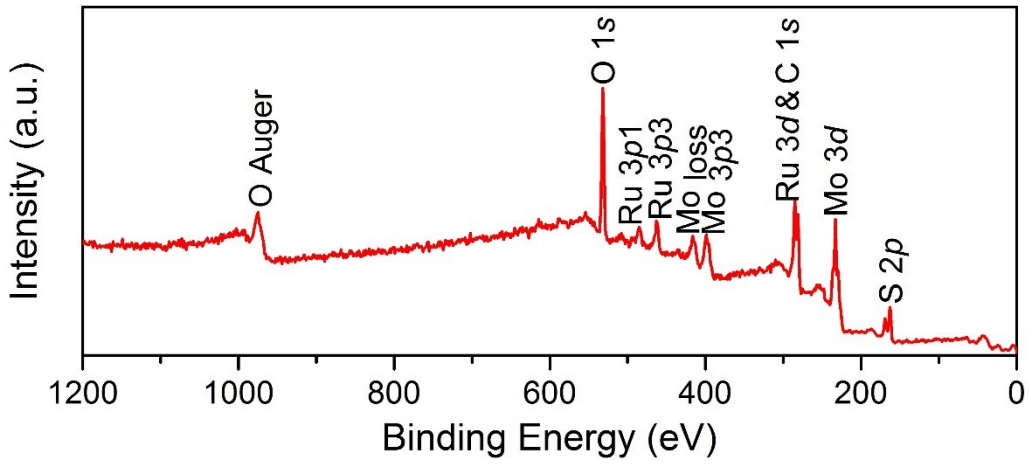

Fig. S6 XPS survey spectrum of Ru/MoS_2/CP.

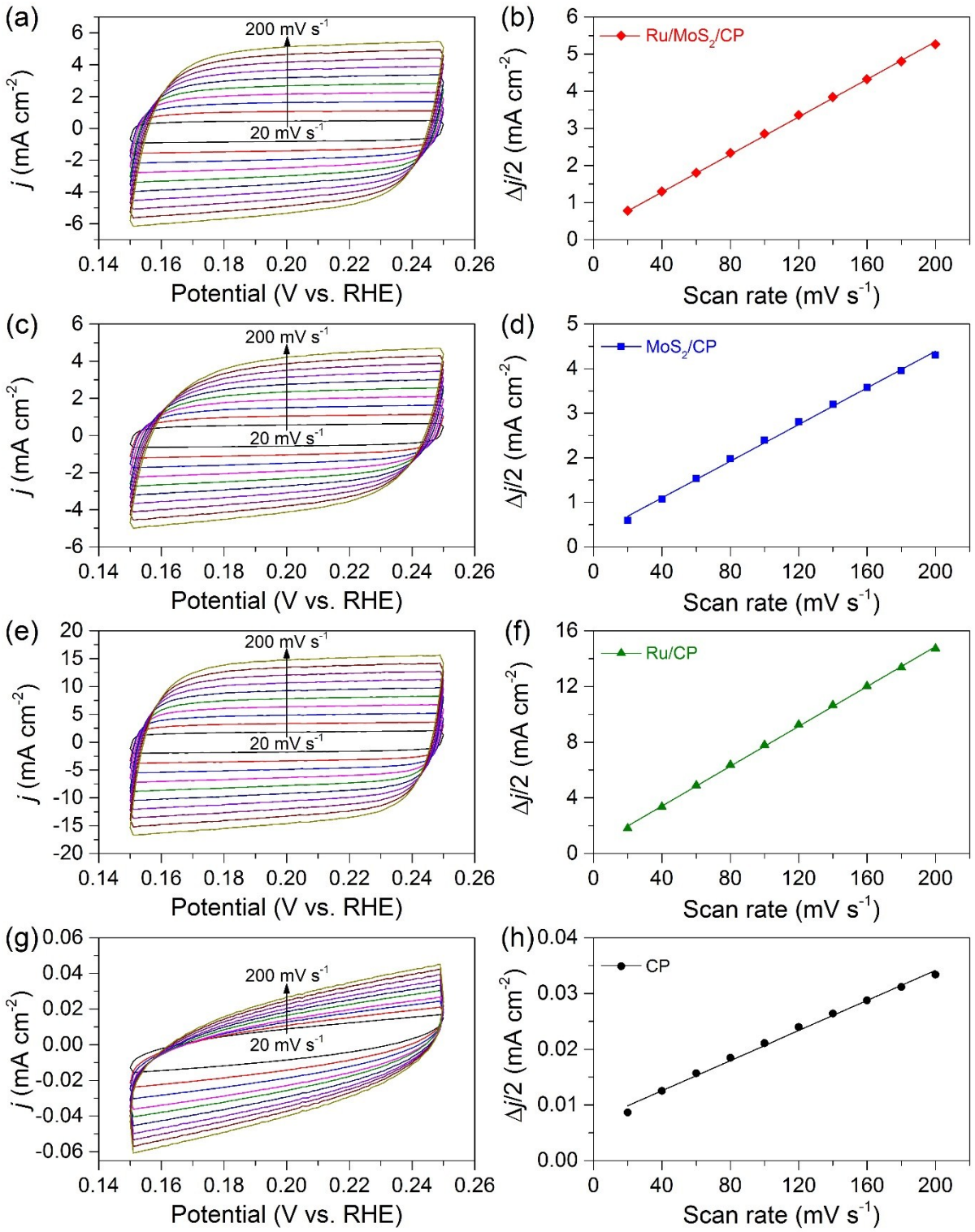

Fig. S7 CV curves and corresponding capacitive current densities at +0.20 V vs. RHE against scan rate for Ru/MoS_2/CP (a,b), MoS_2/CP (c,d), Ru/CP (e,f) and CP (g,h).

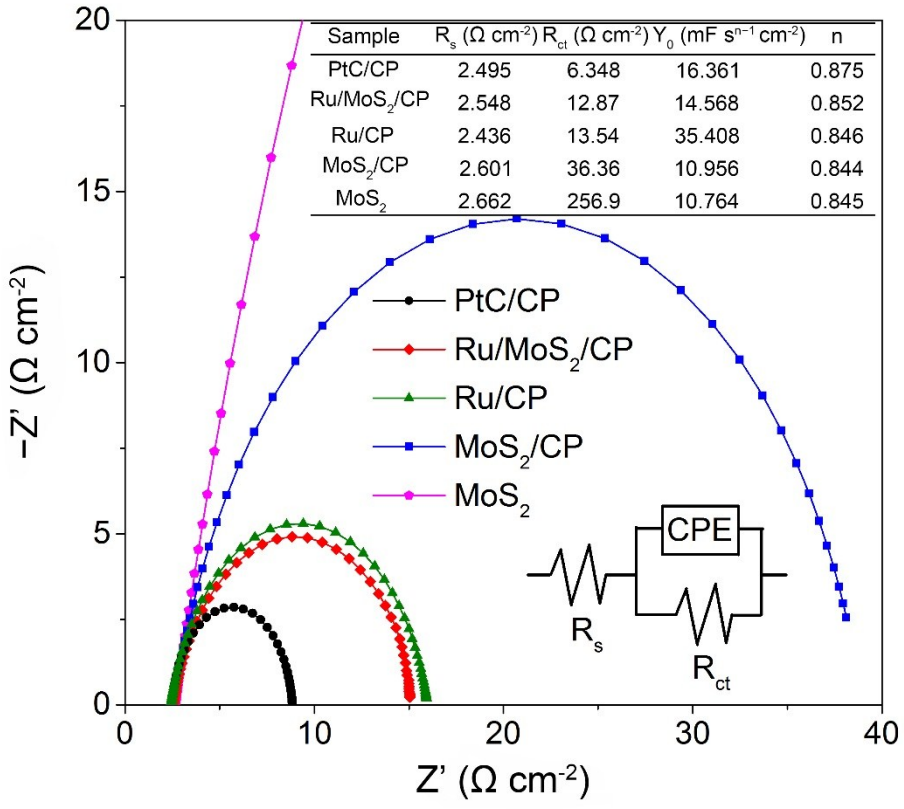

Fig. S8 Nyquist plots for Ru/MoS_2/CP, PtC/CP, Ru/CP, MoS_2/CP, and MoS_2 electrodes, measured at –0.05 V vs. RHE in 1.0 M KOH. Insets are the equivalent circuit and simulated parameters, where R_s, R_{ct}, Y_0 and n are the solution resistance, charge-transfer resistance, and the parameters of a constant phase element (CPE), respectively. The solid lines present the fitted curves.

It was found that bare MoS_2 possesses the highest charge transfer resistance (R_{ct}, up to 256.9 Ω cm^{-2}), as the resistivity through the basal planes is approximately 2200 times higher than along the planes for MoS_2 nanosheets.[2] For MoS_2/CP, the R_{ct} decreases significantly due to the fast electron transfer along CP and the intimate contact between CP and vertically aligned MoS_2 nanosheets. This result is consistent with previous studies.[3,4] Interestingly, Ru/CP displays the smallest R_s, which is likely attributed to the metallic character of Ru and its direct contact with CP. It is clear that Ru/MoS_2/CP exhibits a small R_{ct} of 12.87 Ω cm^{-2}, indicating favourable electrode kinetics for alkaline HER. In addition to the conductive CP framework, the Ru-decoration and O-incorporation ensure better conductivity along and through the planes of the MoS_2 nanosheets.

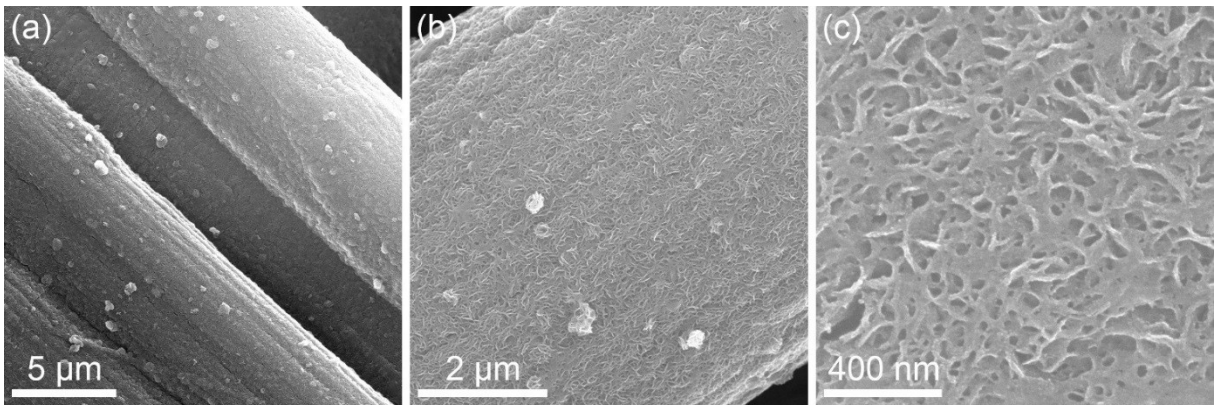

Fig. S9 (a−c) SEM images of Ru/MoS_2/CP electrode after long-term operation.

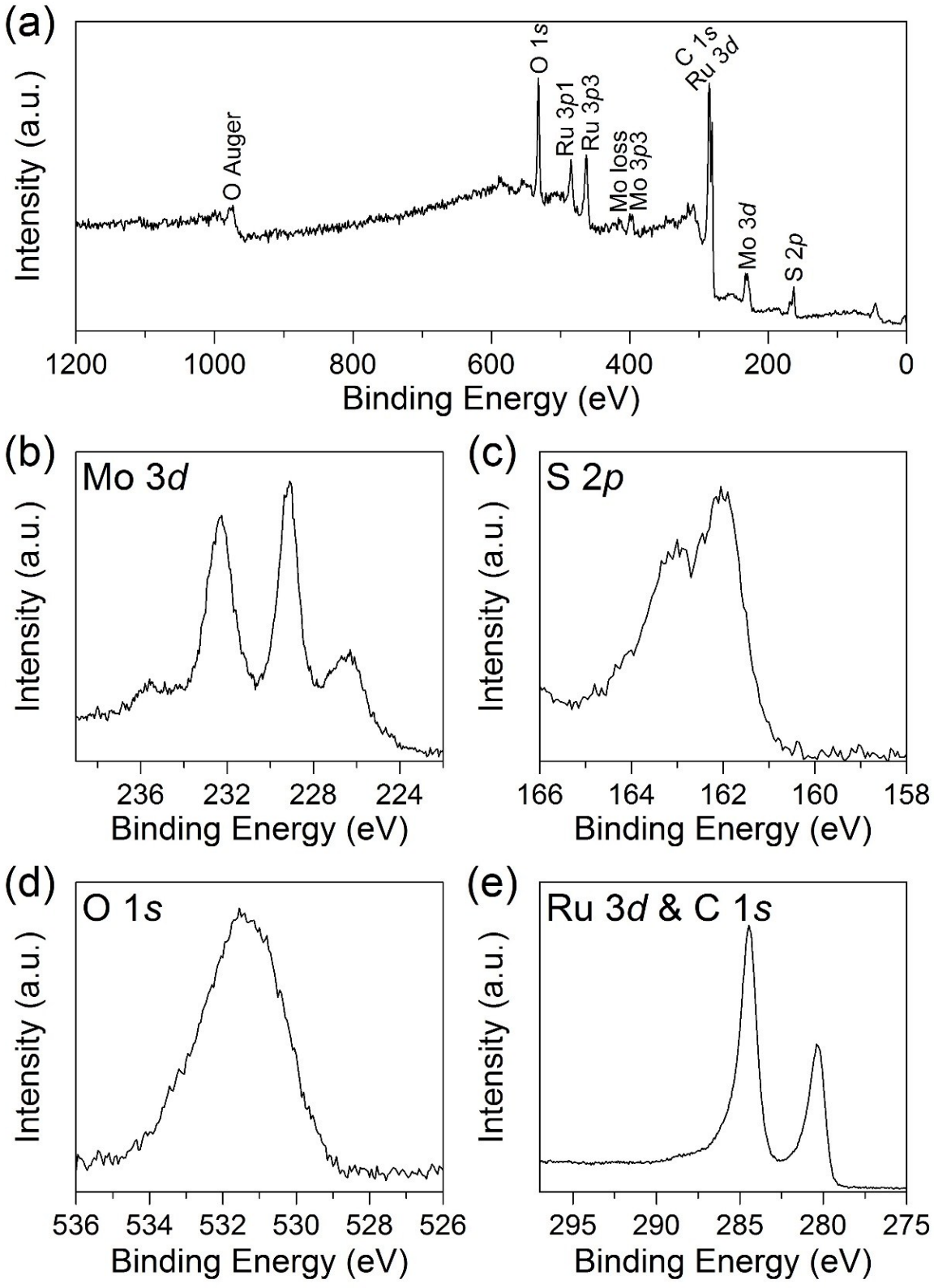

Fig. S10 (a) XPS survey spectrum and high-resolution XPS spectra of (b) Mo 3*d*, (c) S 2*p*, (d) O 1*s*, and (e) Ru 3*d* & C 1*s* of Ru/MoS_2/CP electrode after long-term operation.

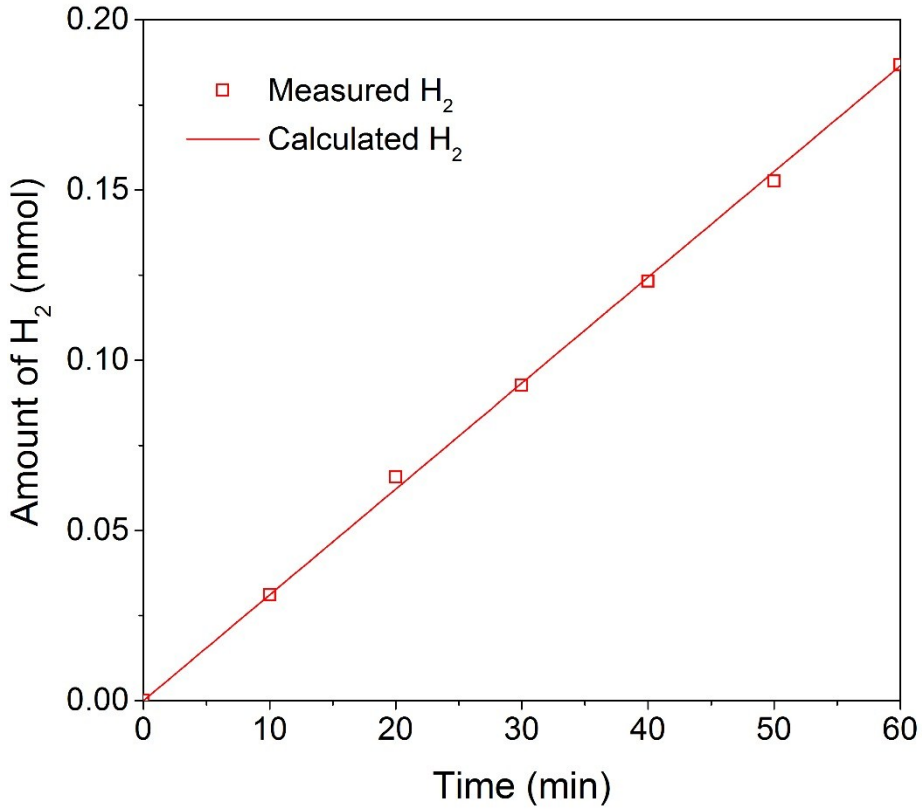

Fig. S11 The amount of H_2 experimentally measured and theoretically calculated versus time for alkaline HER of Ru/MoS_2/CP at a current density of –10 mA cm^{-2}.

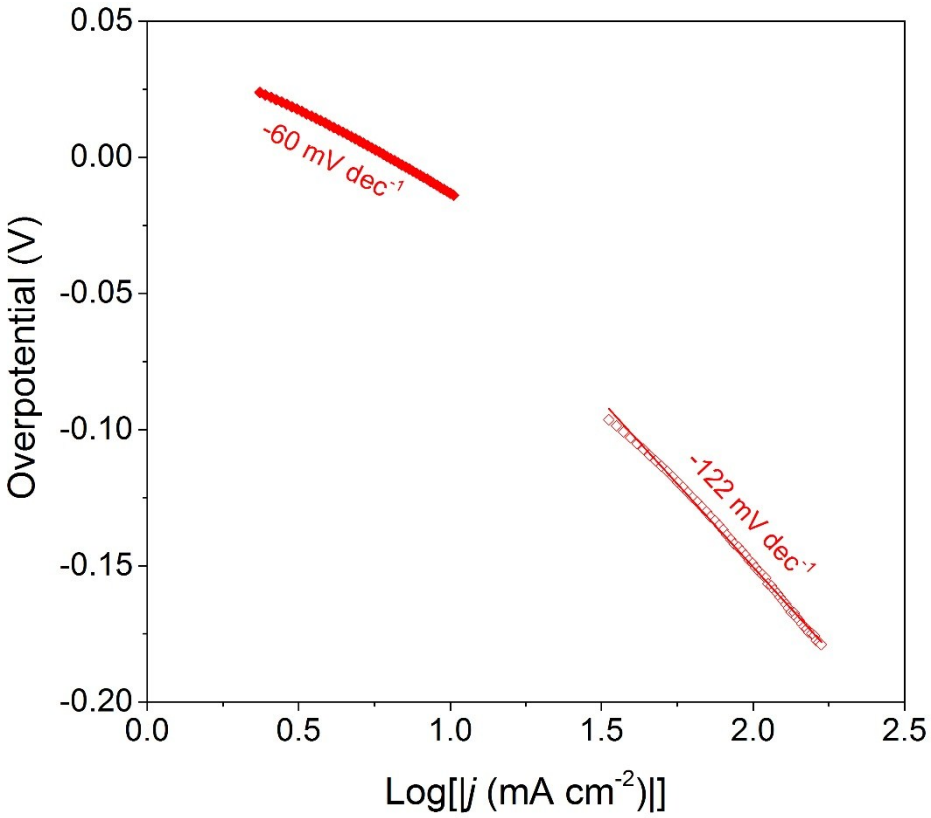

Fig. S12 Tafel plots of Ru/MoS_2/CP at low (solid squares) and high (open squares) potentials.

3. Supplementary Tables

Table S1. Comparison of Ru-based electrocatalysts for HER.

Catalyst	Electrode	Electrolyte	η_{onset} (mV)	η_{10} (mV)	Tafel slope (mV dec^{-1})	Ref.	Year
Ru/MoS_2	Carbon paper	1 M KOH	0	–13	–60	This work	
$Ru@C_2N$	Glassy carbon	1 M KOH	-	–17	–38	5	2017
$Ru\text{-}MoO_2$	Glassy carbon	1 M KOH	-	–29	–31	6	2017
Co-Ru-Pt	Carbon paste	0.5 M H_2SO_4	-	–73.1 @ 4 mA cm^{-2}	–30.4	7	2017
$Ru/C_3N_4/C$	Glassy carbon	1 M KOH	-	–79	-	8	2016
Ru/GLC	Glassy carbon	0.5 M H_2SO_4	–3	–35	–46	9	2016
Ru/SiNW-42.9	Glassy carbon	0.5 M H_2SO_4	-	–200	–81	10	2015
GCE-S-GNs-1000-CB-Ru	Glassy carbon	0.5 M H_2SO_4	0[a]	–75[a]	–61	11	2015

[a] Values estimated from polarization curve found in corresponding Ref.

Table S2. Comparison of MoS_2-based electrocatalysts for HER.

Catalyst	Electrode	Electrolyte	η_{onset} (mV)	η_{10} (mV)	Tafel slope (mV dec^{-1})	Ref.	Year
Ru/MoS_2	Carbon paper	1 M KOH	0	–13	–59.7	This work	
MoS_2-Ni_3S_2 HNRs/NF	Nickel foam	1 M KOH	–31	–98	–61	12	2017
MoS_2|NiS|MoO_3	Ti sheet	1 M KOH	–36	–91	–54.5	13	2017
$(MoS_2)_{0.6}(SnO_2)_{0.4}$/rGO	Glassy carbon	0.5 M H_2SO_4	-	–263±5	–50.8	14	2017
O-MoS2	Carbon cloth	0.5 M H_2SO_4	-	–258	–57	15	2017
$MoS_{2(1-x)}Se_{2x}$(HD)/CNTs	Carbon nanofibers	0.5 M H_2SO_4	–54	–150	–144	16	2017
$Co_2Mo_9S_{26}$	FTO	0.5 M H_2SO_4	-	–260	–64	17	2017
1T/2H MoS_2	Glassy carbon	0.5 M H_2SO_4	-	–234	–46	18	2017
Coral MoS_2@GQDs	Glassy carbon	0.5 M H_2SO_4	–95	–120	–40	19	2017
MoS_2 QDs@GS 3:1	Glassy carbon	0.5 M H_2SO_4	–94	–140	–68	20	2017
C-1TMoS_2	Glassy carbon	0.5 M H_2SO_4	–113	–156	–42.7	21	2017
MoS_2@CNTs-5	Glassy carbon	0.5 M H_2SO_4	-	–62	–49	4	2017
MoS_2/Ni_3S_2	Nickel foam	1 M KOH	–50	–110	–83.1	22	2016
NiS_2-MoS_2	Ti foil	1 M KOH	–76	-	–70	23	2016
MoS_2@Ni/CC	Carbon cloth	1 M KOH	–30	–91	–89	24	2016
HF-MoSP	Glassy carbon	0.5 M H_2SO_4 1 M KOH	–29 –42	–108 –119	–76 –85	25	2016
Pt/MoS_2/CC	Carbon cloth	0.5 M H_2SO_4	0	–18	–49	26	2016
Pt/MoS_2	Mo foil	0.5 M H_2SO_4	-	–60[a]	-	27	2016
N-MoS_2-3	Glassy carbon	0.5 M H_2SO_4	–37	–46	–47	28	2016
Se-GL-MoS_2/G	Glassy carbon	0.5 M H_2SO_4	–102	–185[a]	–50	29	2016
Sn-FL-MoS_2/G	Glassy carbon	0.5 M H_2SO_4	–134	–250[a]	–54	30	2016
Co-MoS_2/G-3	Glassy carbon	0.5 M H_2SO_4	–142	–194	–44.3	31	2016
Cu_7S_4@MoS_2	Glassy carbon	0.5 M H_2SO_4	-	–133	–48	32	2016
CoS_2-MoS_2/CNTs	Glassy carbon	0.5 M H_2SO_4	–70	–180[a]	–67	33	2016
Ni_2P/MoS_2	Glassy carbon	0.5 M H_2SO_4	–75	–190[a]	–76	34	2016
MoS_2-W3	Glassy carbon	0.5 M H_2SO_4	–200	–260	–45.1	35	2016
Co-FL-MoS_2/NG	Glassy carbon	0.5 M H_2SO_4	–90	–175[a]	–59	36	2016
MoSSe@rGO	Glassy carbon	0.5 M H_2SO_4	-	–153	–51	37	2016
Ni-MoS_2	Glassy carbon	0.5 M H_2SO_4	–200	–305[a]	–47	38	2016
P-1T-MoS_2	Glassy carbon	0.5 M H_2SO_4	-	–153	–43	39	2016
O-MoS_2/rGO	Glassy carbon	0.5 M H_2SO_4	–100	-	–40	40	2016
MoS_2/N-RGO-180	Glassy carbon	0.5 M H_2SO_4	–5	–56	–41.3	41	2016
$CoMoS_3$	Glassy carbon	0.5 M H_2SO_4	–112	–171	–56.9	42	2016
CoMoS-2-C	Glassy carbon	0.5 M H_2SO_4	–90	–135	–50	43	2015
$MoS_2/CoSe_2$	Glassy carbon	0.5 M H_2SO_4	–11	–68	–36	44	2015

MoS_2 composite (NMP)	Glassy carbon	0.5 M H_2SO_4	–120	–250[a]	–69	45	2015
H-MoS_2	Glassy carbon	0.5 M H_2SO_4	–50	–167	–70	46	2015
Co_9S_8@MoS_2/CNFs	Glassy carbon	0.5 M H_2SO_4	–64	–190	–110	47	2015
$[Mo_2S_{12}]^{2-}$	Glassy carbon	0.5 M H_2SO_4	-	–161	–39	48	2015
Se-doped MoS_2	Glassy carbon	0.5 M H_2SO_4	–140	–280[a]	–55	49	2015
IF-$Re_xMo_{1-x}S_2$	Glassy carbon	0.5 M H_2SO_4	–70	–250	–136	50	2015
Pt-MoS_2	Glassy carbon	0.1 M H_2SO_4	-	–140[a]	–96	51	2015
CoS_2@MoS_2	Ti foil	0.5 M H_2SO_4	–44	–110.5	–57.3	52	2015
ET&IE MoS_2	Glassy carbon	0.5 M H_2SO_4	–103	–149	–49	53	2015
NG-Mo	Graphene film	0.1 M H_2SO_4	-	–140.6	–105	54	2015
MoS_2 QDs	Glassy carbon	0.5 M H_2SO_4	–210	–300[a]	–60	55	2015
MWCNTs@Cu@MoS_2	Glassy carbon	0.5 M H_2SO_4	–146	–184	–62	56	2015
MoS_x-NCNT	Glassy carbon	0.5 M H_2SO_4	–75	–110	–40	57	2014
MoP|S	Ti foil	0.5 M H_2SO_4	-	–64	–50	58	2014
MoS_2 film	Ti foil	0.5 M H_2SO_4	–150	-	–51	59	2014
1 L MoS_2@NPG	Nanoporous Au	0.5 M H_2SO_4	–118	–226	–46	60	2014
O-MoS_2 (S 180)	Glassy carbon	0.5 M H_2SO_4	–120	–180[a]	–55	1	2013
1T-MoS_2	Glassy carbon	0.5 M H_2SO_4	-	–187	–43	61	2013
MoS_2/RGO	Glassy carbon	0.5 M H_2SO_4	-	–150[a]	–41	62	2011

[a] Values estimated from polarization curves found in corresponding Ref.

4. Supplementary Notes

Supplementary Note 1. Definition of overpotential and Tafel slope

According to classic electrochemistry books,[63,64] the overpotential (η) is defined as the difference between the actual applied potential (E) and the reversible potential (E_r) of the reaction:

$\eta = E - E_r$

For the HER, E_r is 0 V vs. RHE. As a result, HER η equals to the actual applied potential E, which is always a negative quantity. Moreover, according to the Tafel equation ($\eta = a + b \cdot \log|j|$), the HER Tafel slope b determined from the Tafel plot (η vs. $\log|j|$) should also be negative. Note that presenting the data in this way is consistent with electrochemistry conventions.

Note that much of the literature have not paid attention to the definitions and reported HER η and Tafel slope in absolute values. To practice correct notations, the electrochemistry research community should adopt the strict attitude towards electrochemical quantities.

Supplementary Note 2. Double-layer capacitance, roughness factor, and intrinsic alkaline HER activity

Sample	C_{dl} (mF cm^{-2})[a]	R_f[b]	j @ –0.05 V vs. RHE (mA cm^{-2})	$j_{specific}$ @ –0.05 V vs. RHE (μA cm^{-2})[c]
Ru/MoS_2/CP	25	416.7	–31.98	–76.75
Ru/CP	71.6	1193.3	–19.22	–16.11
MoS_2/CP	20.6	343.3	–1.93	–5.62

[a] C_{dl} is estimated by applying the equation: $C_{dl} = \frac{\Delta j}{2 \cdot v} = \frac{(j_a - j_c)}{2 \cdot v}$,[65] where j_a and j_c are the anodic and cathodic current density, respectively, recorded at a potential of +0.20 V vs. RHE, and v is the scan rate (Fig. S7).

[b] According to the Ref. 66, an ideal plane electrode has a C_{dl} of 60 μF cm^{-2}, and R_f can be calculated using the equation: $R_f = \frac{C_{dl}}{60} \times 1000$.

[c] According to the Ref. 67 and 68, $j_{specific}$ is calculated by the equation: $j_{specific} = \frac{j}{R_f}$, where j is the HER current density at a potential of –0.05 V vs. RHE.

Supplementary Note 3. C_{dl} measured by EIS

The parameters (i.e., R_s, R_{ct}, Y_0, and n) from the EIS measurement using the applied equivalent circuit can be used to calculate C_{dl} according to the following equation:[65,68–70]

$$C_{dl} = [Y_0(\frac{1}{R_s} + \frac{1}{R_{ct}})^{(n-1)}]^{\frac{1}{n}}$$

As shown in the below table, the C_{dl} values estimated by EIS match well with those obtained from the scan rate-dependent CVs (within an error range of ±10%).

Sample	R_s (Ω cm^{-2})	R_{ct} (Ω cm^{-2})	Y_0 (mF s^{n-1} cm^{-2})	n	C_{dl} (mF cm^{-2})
Ru/MoS_2/CP	2.548	12.87	14.568	0.852	26.45
Ru/CP	2.436	13.54	35.408	0.846	77.34
MoS_2/CP	2.601	36.36	10.956	0.844	20.09

Supplementary Note 4. HER mechanism and Tafel slope

Regarding the HER mechanism, two possible reaction pathways have been proposed.[71,72] (i) The first step is to form electrochemically adsorbed hydrogen (H_{ads}, Volmer reaction):

$H^+ + e^- \rightleftharpoons H_{ads}$ (in acidic solution)

$H_2O + e^- \rightleftharpoons H_{ads} + OH^-$ (in alkaline solution)

$$b = \frac{-2.303 \cdot R \cdot T}{\beta \cdot F} \approx -120\ mV\ dec^{-1}$$

where R is the ideal gas constant, T is the absolute temperature, β ≈ 0.5 is the symmetry coefficient, and F is the Faraday constant.

A different reaction step in the next pathway leads to a different HER mechanism. To be specific, (ii) the formed H_{ads} undergoes an electrochemical desorption step (Heyrovsky reaction):

$H_{ads} + H^+ + e^- \rightleftharpoons H_2$ (in acidic solution)

$H_{ads} + H_2O + e^- \rightleftharpoons H_2 + OH^-$ (in alkaline solution)

$$b = \frac{-2.303 \cdot R \cdot T}{(1+\beta) \cdot F} \approx -40\ mV\ dec^{-1}$$

or a recombination step (Tafel reaction)

$H_{ads} + H_{ads} \rightleftharpoons H_2$ (in both acidic and alkaline solutions)

$$b = \frac{-2.303 \cdot R \cdot T}{2 \cdot F} \approx -30\ mV\ dec^{-1}$$

For Ru/MoS_2/CP in this work, its Tafel slope in 1.0 M KOH was found to be −60 mV dec^{-1}. In fact, a Tafel slope of about −60 mV dec^{-1} is commonly observed on Ru-based HER

catalysts.[73–78] It can be explained by a formal kinetics approach in two cases: (i) the Heyrovsky mechanism is operative and the adsorption of the reaction intermediate H_{ads} proceeds under Temkin conditions in the range of intermediate surface coverages $0.2 < \theta < 0.8$;[77,79] (ii) the mechanism involves a surface chemical rearrangement step $H_{ads}(A) \rightarrow H_{ads}(B)$ as the rate-determining step (RDS), which features the surface sites A and B having different energy levels.[68,75,78,79] The latter case supports the proposed hypothesis on the synergy between Ru and MoS_2. Accordingly, the following HER mechanism is predicted:

$$H_2O + e^- \rightleftharpoons H_{ads}(Ru) + OH^- \quad (1)$$

$$H_{ads}(Ru) \rightarrow H_{ads}(Mo) \quad (2)$$

$$H_{ads}(Mo) + H_{ads}(Mo) \rightleftharpoons H_2 \quad (3)$$

If Step 2 representing the surface diffusion of H_{ads} from the Ru sites to the nearby unsaturated Mo atoms of MoS_2 is the RDS, the overall reaction rate is equal to:

$$-j = 2 \cdot F \cdot k_2 \cdot \theta(Ru) \cdot (1 - \theta(MoS_2)) \quad (4)$$

where $k_{\pm i}$ is the rate constant of step i in the forward (+) or backward (–) direction and θ the fractional occupancy of H-adsorption sites on Ru or MoS_2. If we assume that the Volmer step (Step 1) preceding the RDS is in quasi-equilibrium at low overpotentials, we obtain the following equation:

$$k_1 \cdot (1 - \theta(Ru)) \cdot e^{-\frac{\beta_1 \cdot F \cdot E}{R \cdot T}} = k_{-1} \cdot c(OH^-) \cdot \theta(Ru) \cdot e^{\frac{(1-\beta_1) \cdot F \cdot E}{R \cdot T}} \quad (5)$$

where β is the symmetry factor. Since θ(Ru) is close to 0 at low overpotentials, it can be approximated that $(1–\theta(Ru)) \rightarrow 1$. In that case from Eq. 5, we obtain:

$$\theta(Ru) = \frac{k_1}{k_{-1}} \cdot \frac{1}{c(OH^-)} \cdot e^{-\frac{F \cdot E}{R \cdot T}} \quad (6)$$

Now, by replacing θ(Ru) in the rate law of the total reaction (Eq. 4), we get:

$$-j = 2 \cdot F \cdot k_2 \cdot \frac{k_1}{k_{-1}} \cdot \frac{1}{c(OH^-)} \cdot e^{-\frac{F \cdot E}{R \cdot T}} \quad (7)$$

For T = 298 K, the Tafel slope is:

$$b = -\frac{2.303 \cdot R \cdot T}{F} = -60\ mV\ dec^{-1} \quad (8)$$

Given that the theoretical Tafel slope is identical to the observed one on Ru/MoS_2/CP (−60 mV dec^{-1}), such a result further supports the interfacial synergy between Ru and MoS_2 towards improve alkaline HER kinetics.

Notably, the aforementioned mechanism could apply to Ru/MoS_2/CP only at low overpotentials when $\theta \rightarrow 0$ (at overpotentials lower than −25 mV according to Fig. 3b). At higher overpotentials, i.e. at higher current densities, where $\theta \rightarrow 1$, the reaction pathway involving Step 2 as the RDS reaches a reaction limiting current density,[79] and H desorption from the Ru sites dominantly proceeds through the Heyrovsky step:

$$H_{ads}(Ru) + H_2O + e^- = H_2 + OH^- \quad (9)$$

Under such conditions, the overall reaction rate is then given by:

$$-j = 2 \cdot F \cdot k_2 \cdot e^{-\frac{\beta_1 \cdot F \cdot E}{R \cdot T}} \quad (10)$$

For T = 298 K, assuming $\beta_1 = 0.5$, the theoretical Tafel slope is:

$$b = -\frac{2.303 \cdot R \cdot T}{\beta_1 \cdot F} = -120\ mV\ dec^{-1} \quad (11)$$

To this end, we also calculated the Tafel slope of Ru/MoS_2/CP at higher overpotentials, as presented in Fig. S12. A Tafel slope of −122 mV dec^{-1} is observed on Ru/MoS_2/CP at high overpotentials, which is also consistent with the theoretically calculated slope. All these results further demonstrate the proposed alkaline HER mechanism on Ru/MoS_2/CP.

5. Supplementary Movie

Movie S1. The self-supported Ru/MoS_2/CP electrode is directly employed as the working electrode in a typical three-electrode cell setup using 1.0 M KOH as the electrolyte. H_2 bubbles are visibly observed on the Ru/MoS_2/CP electrode at an overpotential of −15 mV. When the overpotential increases from −15 to −100 mV, the evolution rate of H_2 bubbles increases significantly, and the generated bubbles release quickly without obvious adherence on the electrode. No visible peeling of the active material from the electrode can be observed, reflecting remarkable structural robustness of the as-synthesized electrode.

6. References

1 J. Xie, J. Zhang, S. Li, F. Grote, X. Zhang, H. Zhang, R. Wang, Y. Lei, B. Pan and Y. Xie, *J. Am. Chem. Soc.*, 2013, **135**, 17881−17888.

2 H. Tributsch, *Ber. Bunsen-Ges.*, 1977, **81**, 361−369.

3 H. Yu, X. Yu, Y. Chen, S. Zhang, P. Gao and C. Li, *Nanoscale*, 2015, **7**, 8731−8738.

4 A. Li, Y. Hu, M. Yu, X. Liu and M. Li, *Int. J. Hydrogen Energy*, 2017, **42**, 9419−9427.

5 J. Mahmood, F. Li, S. M. Jung, M. S. Okyay, I. Ahmad, S. J. Kim, N. Park, H. Y. Jeong and J. B. Baek, *Nat. Nanotechnol.*, 2017, **12**, 441−446.

6 P. Jiang, Y. Yang, R. Shi, G. Xia, J. Chen, J. Su and Q. Chen, *J. Mater. Chem. A*, 2017, **5**, 5475−5485.

7 J. V. Medina-Flores, A. Manzo-Robledo, J. M. Mora-Hernández and E. M. Arce Estrada, *Int. J. Hydrogen Energy*, 2017, **42**, 38−45.

8 Y. Zheng, Y. Jiao, Y. Zhu, L. H. Li, Y. Han, Y. Chen, M. Jaroniec and S. Z. Qiao, *J. Am. Chem. Soc.*, 2016, **138**, 16174−16181.

9 Z. Chen, J. Lu, Y. Ai, Y. Ji, T. Adschiri and L. Wan, *ACS Appl. Mater. Interfaces*, 2016, **8**, 35132−35137.

10 L. Zhu, Q. Cai, F. Liao, M. Sheng, B. Wu and M. Shao, *Electrochem. Commun.*, 2015, **52**, 29−33.

11 R. K. Shervedani and A. Amini, *Carbon*, 2015, **93**, 762−773.

12 Y. Yang, K. Zhang, H. Lin, X. Li, H. C. Chan, L. Yang and Q. Gao, *ACS Catal.*, 2017, **7**, 2357−2366.

13 C. Wang, B. Tian, M. Wu and J. Wang, *ACS Appl. Mater. Interfaces*, 2017, **9**, 7084−7090.

14 S. Ravula, C. Zhang, J. B. Essner, J. D. Robertson, J. Lin and G. A. Baker, *ACS Appl. Mater. Interfaces*, 2017, **9**, 8065−8074.

15 X. Shang, W. H. Hu, X. Li, B. Dong, Y. R. Liu, G. Q. Han, Y. M. Chai and C. G. Liu, *Electrochim. Acta*, 2017, **224**, 25−31.

16 H. Yang, T. Zhang, H. Zhu, M. Zhang, W. Wu and M. Du, *Int. J. Hydrogen Energy*, 2017, **42**, 1912−1918.

17 I. Roger, R. Moca, H. N. Miras, K. G. Crawford, D. A. J. Moran, A. Y. Ganin and M. D. Symes, *J. Mater. Chem. A*, 2017, **5**, 1472−1480.

18 D. Wang, X. Zhang, S. Bao, Z. Zhang, H. Fei and Z. Wu, *J. Mater. Chem. A*, 2017, **5**, 2681−2688.

19 B. Guo, K. Yu, H. Li, R. Qi, Y. Zhang, H. Song, Z. Tang, Z. Zhu and M. Chen, *ACS Appl. Mater. Interfaces*, 2017, **9**, 3653−3660.

20 W. Li, F. Li, X. Wang, Y. Tang, Y. Yang, W. Gao and R. Li, *Appl. Surf. Sci.*, 2017, **401**, 190−197.

21 Y. Li, L. Wang, S. Zhang, X. Dong, Y. Song, T. Cai and Y. Liu, *Catal. Sci. Technol.*, 2017, **7**, 718−724.

22 J. Zhang, T. Wang, D. Pohl, B. Rellinghaus, R. Dong, S. Liu, X. Zhuang and X. Feng, *Angew. Chem. Int. Ed.*, 2016, **55**, 6702−6707.

23 T. An, Y. Wang, J. Tang, W. Wei, X. Cui, A. M. Alenizi, L. Zhang and G. Zheng, *J. Mater. Chem. A*, 2016, **4**, 13439−13443.

24 Z. Xing, X. Yang, A. M. Asiri and X. Sun, *ACS Appl. Mater. Interfaces*, 2016, **8**, 14521−14526.

25 A. Wu, C. Tian, H. Yan, Y. Jiao, Q. Yan, G. Yang and H. Fu, *Nanoscale*, 2016, **8**, 11052−11059.

26 Y. Luo, D. Huang, M. Li, X. Xiao, W. Shi, M. Wang, J. Su and Y. Shen, *Electrochim. Acta*, 2016, **219**, 187−193.

27 A. Jagminas, A. Naujokaitis, R. Žalnėravičius, V. Jasulaitiene and G. Valušis, *Appl. Surf. Sci.*, 2016, **385**, 56−62.

28 W. Xiao, P. Liu, J. Zhang, W. Song, Y. P. Feng, D. Gao and J. Ding, *Adv. Energy Mater.*, 2017, **7**, 1602086.

29 L. Ma, L. Xu, W. Lin, Q. Li, X. Xu, X. Zhou and H. Li, *Adv. Powder Technol.*, 2016, **27**, 2153−2160.

30 L. Ma, L. Xu, X. Zhou, X. Xu, J. Luo and L. Zhang, *Colloids Surf. A*, 2016, **509**, 140−148.

31 J. Ye, W. Chen, S. Xu, Z. Yu and S. Hou, *RSC Adv.*, 2016, **6**, 104925−104932.

32 J. Xu, J. Cui, C. Guo, Z. Zhao, R. Jiang, S. Xu, Z. Zhuang, Y. Huang, L. Wang and Y. Li, *Angew. Chem. Int. Ed.*, 2016, **55**, 6502−6505.

33 Y. R. Liu, W. H. Hu, X. Li, B. Dong, X. Shang, G. Q. Han, Y. M. Chai, Y. Q. Liu and C. G. Liu, *Appl. Surf. Sci.*, 2016, **384**, 51−57.

34 Y. R. Liu, W. H. Hu, X. Li, B. Dong, X. Shang, G. Q. Han, Y. M. Chai, Y. Q. Liu and C. G. Liu, *Appl. Surf. Sci.*, 2016, **383**, 276−282.

35 J. N. He, Y. Q. Liang, J. Mao, X. M. Zhang, X. J. Yang, Z. D. Cui, S. L. Zhu, Z. Y. Li and B. B. Li, *J. Electrochem. Soc.*, 2016, **163**, H299−H304.

36 L. Ma, L. Xu, X. Xu, X. Zhou, J. Luo and L. Zhang, *Mater. Sci. Eng. B*, 2016, **212**, 30−38.

37 B. Konkena, J. Masa, W. Xia, M. Muhler and W. Schuhmann, *Nano Energy*, 2016, **29**, 46−53.

38 D. Wang, X. Zhang, Y. Shen and Z. Wu, *RSC Adv.*, 2016, **6**, 16656−16661.

39 Y. Yin, J. Han, Y. Zhang, X. Zhang, P. Xu, Q. Yuan, L. Samad, X. Wang, Y. Wang, Z. Zhang, P. Zhang, X. Cao, B. Song and S. Jin, *J. Am. Chem. Soc.*, 2016, **138**, 7965−7972.

40 A. Liu, L. Zhao, J. Zhang, L. Lin and H. Wu, *ACS Appl. Mater. Interfaces*, 2016, **8**, 25210−25218.

41 Y. J. Tang, Y. Wang, X. L. Wang, S. L. Li, W. Huang, L. Z. Dong, C. H. Liu, Y. F. Li and Y. Q. Lan, *Adv. Energy Mater.*, 2016, **6**, 1600116.

42 L. Yu, B. Y. Xia, X. Wang and X. W. Lou, *Adv. Mater.*, 2016, **28**, 92−97.

43 X. Dai, K. Du, Z. Li, M. Liu, Y. Ma, H. Sun, X. Zhang and Y. Yang, *ACS Appl. Mater. Interfaces*, 2015, **7**, 27242−27253.

44 M. R. Gao, J. X. Liang, Y. R. Zheng, Y. F. Xu, J. Jiang, Q. Gao, J. Li and S. H. Yu, *Nat. Commun.*, 2015, **6**, 5982.

45 S. Xu, D. Li and P. Wu, *Adv. Funct. Mater.*, 2015, **25**, 1127−1136.

46 J. Zhang, S. Liu, H. Liang, R. Dong and X. Feng, *Adv. Mater.*, 2015, **27**, 7426−7431.

47 H. Zhu, J. Zhang, R. Yanzhang, M. Du, Q. Wang, G. Gao, J. Wu, G. Wu, M. Zhang, B. Liu, J. Yao and X. Zhang, *Adv. Mater.*, 2015, **27**, 4752−4759.

48 Z. Huang, W. Luo, L. Ma, M. Yu, X. Ren, M. He, S. Polen, K. Click, B. Garrett, J. Lu, K. Amine, C. Hadad, W. Chen, A. Asthagiri and Y. Wu, *Angew. Chem. Int. Ed.*, 2015, **54**, 15181−15185.

49 X. Ren, Q. Ma, H. Fan, L. Pang, Y. Zhang, Y. Yao, X. Ren and S. Liu, *Chem. Commun.*, 2015, **51**, 15997−16000.

50 M. Chhetri, U. Gupta, L. Yadgarov, R. Rosentsveig, R. Tenne and C. N. R. Rao, *Dalton Trans.*, 2015, **44**, 16399−16404.

51 J. Deng, H. Li, J. Xiao, Y. Tu, D. Deng, H. Yang, H. Tian, J. Li, P. Ren and X. Bao, *Energy Environ. Sci.*, 2015, **8**, 1594−1601.

52 H. Zhang, Y. Li, T. Xu, J. Wang, Z. Huo, P. Wan and X. Sun, *J. Mater. Chem. A*, 2015, **3**, 15020−15023.

53 M. R. Gao, M. K. Y. Chan and Y. Sun, *Nat. Commun.*, 2015, **6**, 7493.

54 S. Chen, J. Duan, Y. Tang, B. Jin and S. Z. Qiao, *Nano Energy*, 2015, **11**, 11−18.

55 D. Gopalakrishnan, D. Damien, B. Li, H. Gullappalli, V. K. Pillai, P. M. Ajayan and M. M. Shaijumon, *Chem. Commun.*, 2015, **51**, 6293−6296.

56 F. Li, J. Li, X. Lin, X. Li, Y. Fang, L. Jiao, X. An, Y. Fu, J. Jin and R. Li, *J. Power Sources*, 2015, **300**, 301−308.

57 D. J. Li, U. N. Maiti, J. Lim, D. S. Choi, W. J. Lee, Y. Oh, G. Y. Lee and S. O. Kim, *Nano Lett.*, 2014, **14**, 1228−1233.

58 J. Kibsgaard and T. F. Jaramillo, *Angew. Chem. Int. Ed.*, 2014, **53**, 14433−14437.

59 Z. Lu, W. Zhu, X. Yu, H. Zhang, Y. Li, X. Sun, X. Wang, H. Wang, J. Wang, J. Luo, X. Lei and L. Jiang, *Adv. Mater.*, 2014, **26**, 2683−2687.

60 Y. Tan, P. Liu, L. Chen, W. Cong, Y. Ito, J. Han, X. Guo, Z. Tang, T. Fujita, A. Hirata and M. W. Chen, *Adv. Mater.*, 2014, **26**, 8023−8028.

61 M. A. Lukowski, A. S. Daniel, F. Meng, A. Forticaux, L. Li and S. Jin, *J. Am. Chem. Soc.*, 2013, **135**, 10274−10277.

62 Y. Li, H. Wang, L. Xie, Y. Liang, G. Hong and H. Dai, *J. Am. Chem. Soc.*, 2011, **133**, 7296−7299.

63 E. Gileadi, *Electrode Kinectics for Chemists, Chemical Engineers and Materials Scientists*, Wiley-VCH, New York, 1993.

64 A. J. Bard and L. R. Faulkner, *Electrochemical Methods: Fundamentals and Applications*, Wiley, New York, 2rd Edition, 2000.

65 C. C. L. McCrory, S. Jung, J. C. Peters and T. F. Jaramillo, *J. Am. Chem. Soc.*, 2013, **135**, 16977−16987.

66 S. Levine and A. L. Smith, *Discuss. Faraday Soc.*, 1971, **52**, 290−301.

67 B. M. Jović, V. D. Jović, U. Č. Lačnjevac, L. Gajić-Krstajić and N. V. Krstajić, *Int. J. Hydrogen Energy*, 2015, **40**, 10480−10490.

68 B. M. Jović, V. D. Jović, U. Č. Lačnjevac, S. I. Stevanović, J. Kovač, M. Radović and N. V. Krstajić, *J. Electroanal. Chem.*, 2016, **766**, 78−86.

69 G. J. Brug, A. L. G. van den Eeden, M. Sluyters-Rehbach and J. H. Sluyters, *J. Electroanal. Chem. Interfacial Electrochem.*, 1984, **176**, 275−295.

70 D. Lin and A. Lasia, *J. Electroanal. Chem.*, 2017, **785**, 190−195.

71 B. E. Conway and B. V. Tilak, *Electrochim. Acta*, 2002, **47**, 3571−3594.

72 Y. Zheng, Y. Jiao, M. Jaroniec and S. Z. Qiao, *Angew. Chem. Int. Ed.*, 2015, **54**, 52−65.

73 M. Fleischmann and M. Grenness, *J. Chem. Soc., Faraday Trans. 1*, 1972, **68**, 2305−2315.

74 V. S. Bagotzky, A. M. Skundin and E. K. Tuseeva, *Electrochim. Acta*, 1976, **21**, 29−36.

75 I. M. Kodintsev and S. Trasatti, *Electrochim. Acta*, 1994, **39**, 1803−1808.

76 A. C. Tavares and S. Trasatti, *Electrochim. Acta*, 2000, **45**, 4195−4202.

77 U. Č. Lačnjevac, B. M. Jović, V. D. Jović, V. R. Radmilović and N. V. Krstajić, *Int. J. Hydrogen Energy*, 2013, **38**, 10178−10190.

78 U. Č. Lačnjevac, V. V. Radmilović, V. R. Radmilović and N. V. Krstajić, *Electrochim. Acta*, 2015, **168**, 178−190.

79 A. Kahyarian, B. Brown and S. Nesic, *J. Electrochem. Soc.*, 2017, **164**, H365−H374.